Applied Catalysis B: Environmental 100 (2010) 31–41

Contents lists available at ScienceDirect

Applied Catalysis B: Environmental

journal homepage: www.elsevier.com/locate/apcatb

Kinetic modeling of sulfur poisoning and regeneration of lean NO_x traps

Louise Olsson[a,*], Marielle Fredriksson[a], Richard J. Blint[b]

[a] Chemical Engineering and Competence Centre for Catalysis, Chalmers University of Technology, SE- 412 96 Göteborg, Sweden
[b] General Motors R&D Center, Chemical and Environmental Sciences Laboratory, 30500 Mound Rd, Warren, MI 48090-9055, United States

ARTICLE INFO

Article history:
Received 23 March 2010
Received in revised form 30 June 2010
Accepted 6 July 2010
Available online 15 July 2010

Keywords:
Catalyst deactivation
Kinetic modeling
Lean NO_x traps
NO_x storage
SO_2
Sulfur poisoning and regeneration

ABSTRACT

Sulfur poisoning and regeneration of lean NO_x traps were investigated using experiments and kinetic modeling. A commercial Pt, Rh and barium containing NO_x storage catalyst was used. The catalyst also contained oxygen storage material. First the oxygen storage capacity (OSC) was investigated using steps with oxygen and hydrogen. The OSC was substantial with a total use of all hydrogen (1%) for about 20 s. The results were similar at the three investigated temperatures (300, 400 and 500 °C), indicating that it is a low activation barrier connected with the process. Further, no effect was observed when adding 15 ppm SO_2 to the feed. Since no SO_2 was observed in the outlet it is possible that SO_2 is adsorbed during the lean period and then reduced to form H_2S in the rich period (not measured). Further, the NO_x storage was found to decrease during SO_2 exposure, and the decrease was linear and dose dependent. In addition, we investigated different regeneration strategies. When using 500 ppm H_2 for 60 min at 700 °C the regeneration was poor. However, when adding 5% CO_2 to the 500 ppm H_2 the regeneration was increased drastically. Further, the regeneration was decreased when decreasing the temperature to 600 °C, and further decreased when using 500 °C. In addition, it was beneficial with increasing the hydrogen concentration. The kinetic model contains three sub-models: (i) NO_x storage and regeneration, (ii) oxygen storage and reduction and (iii) sulfur poisoning and sulfur regeneration. It was crucial to add NO_x storage on two sites; barium and alumina. The NO_x adsorbed on alumina is more loosely bound. Further, in the model formation of sulfates were added on both components. This was important in order to describe the rate of the sulfur deactivation. If sulfur was adsorbed only on barium the deactivation would have been too rapid. The model could describe the experimental features well.

1. Introduction

Diesel and lean burn gasoline engines have a lower fuel consumption compared to conventional stoichiometric gasoline engines. However, due to the large oxygen excess in these exhausts it is important to decrease the nitrogen oxides (NO_x) emissions due to environmental reasons, since the standard three-way catalyst (TWC) will be oxygen poisoned. One concept is lean NO_x traps (LNT), also called NO_x storage and reduction (NSR) and lean NO_x adsorbers (LNA). The engine is altered between lean (oxygen excess) and rich (fuel excess) operation. During the lean period the catalyst stores the NO_x and during the rich periods the NO_x is release and reduced on the noble metal sites. Several studies have shown that sulfur poisons the NO_x storage capacity using several experimental techniques like flow reactor experiments [1,2], in situ FTIR [3–6], X-ray photo emission spectroscopy (XPS) [1,7], X-ray absorption spectroscopy (EXAFS) [5], temperature programmed desorption (TPD) [8], X-ray diffraction (XRD) [9] and energy dispersive X-ray spectroscopic (EDX) [9]. It is observed that the deactivation of the NO_x storage capacity is proportional to the total SO_2 dose and is not affected by the SO_2 concentration [1]. Further, deactivation was larger when SO_2 was present in the rich condition compared to in the lean period [10]. Corbos et al. [11] observed close to complete regeneration in rich conditions at 550 °C. Further, Poulston and Rajaram [7] found that the sulfur regeneration was increased when CO_2 was present.

There are some kinetic models present in the literature for lean NO_x traps. Olsson et al. [12,13] and Tuttlies et al. [14] use a shrinking core type of model for describing mass-transport resistance within the barium particles. Scholz et al. [15] presented a global reaction kinetic model based on a multiple storage site mechanism using hydrogen as reducing agent. However, the ammonia production was not included in this model. Laurent et al. [16] presented a global model for NO_x storage and Koci et al. [17] presented a kinetic model for NO_x storage and regeneration using hydrogen including ammonia formation. Bhatia et al. [18] presents a two sites global kinetic model for NO_x storage and reduction, using H_2 as reducing agent. In a recent publication Koci et al. [19] presents a model that can describe the effect of using different reducing agents. A series of papers by Olsson and co-workers describe a detailed kinetic

* Corresponding author. Fax: +46 31 772 3035.
E-mail address: louise.olsson@chalmers.se (L. Olsson).

0926-3373/$ – see front matter © 2010 Elsevier B.V. All rights reserved.
doi:10.1016/j.apcatb.2010.07.004

Nomenclature

Parameter

a_j	active site density for reaction j (mol-sites/m^3)
A	pre-exponential factor (Unit depends on rate expression. The concentrations in the rates are in mol/m^3 and the rates in unit s^{-1}.)
A_{tot}	front area of the monolith (m^2)
$c_{g,tot}$	the total concentration in the gas bulk, where the temperature is T_g (mol/m^3)
$c_{s,i}$	the molar concentration of the gas specie i at the catalyst surface (mol/m^3)
$c_{s,tot}$	the total concentration at the catalyst surface, where the temperature is T_s (mol/m^3)
D_h	hydraulic diameter of channel (m)
$D_{i,m}$	binary diffusion coefficient of specie i in the mixture (m^2/s)
E_a	activation energy (J/mol)
k	rate constant (Unit depends on rate expression. The concentrations in the rates are in mol/m^3 and the rates in unit s^{-1}.)
$k_{m,i}$	mass-transfer coefficient for specie i (mol/(m^2 s))
$n_{cycle,3}$	NO_x storage capacity in cycle 3 (μmol)
Nr	number of reactions
n_{SO_2}	amount of SO_2 exposure per cycle (μmol)
$n_{theoretical}$	theoretical NO_x storage capacity (μmol)
no_{cycles}	number of cycles with SO_2 present
Sh	Sherwood number
P_{tot}	total pressure (Pa)
r_j	reaction rate for reaction j (mol/(mol-sites s))
R	gas constant (J/(mol K))
s_{ij}	stoichiometric coefficient of specie i in reaction j
s_{kj}	stoichiometric coefficient of surface specie k in reaction j
S	surface area per reactor volume (m^{-1})
t	time (s)
T_s	temperature at catalyst surface (K)
w	molar flow rate (mol/s)
$x_{g,i}$	mole fraction of gas specie i
$x_{s,i}$	mole fraction of gas specie i at the surface
z	axial position (m)
α	constant
θ_k	coverage of component k

model for NO_x storage with thermal regeneration [20], propene regeneration [21], hydrogen regeneration including ammonia formation [22] and sulfur poisoning [23]. The kinetic model for sulfur poisoning is developed using sulfur exposure before temperature programmed desorption experiments with NO_2 [23]. However, there are today no kinetic models available that can describe the sulfur poisoning during lean rich cycling and the regeneration of the formed sulfates, which is the objective with this work.

2. Experimental

A commercial NO_x storage catalyst was used in this work. The catalyst contains Pt, Rh, barium and oxygen storage components. The catalyst was aged in a reactor by:

- 750 °C: 5 min stoichiometric and 1 min lean exposures for 1 h. Stoichiometric conditions: 9000 ppm CO, 500 ppm NO, 1100 ppm C_3H_6 and 9200 ppm O_2. Lean conditions: 9000 ppm CO, 500 ppm NO, 1100 ppm C_3H_6 and 8% O_2.
- 850 °C: 1 h in Ar
- Saturation of the sample with sulfur during mixed lean and rich conditions at 400 °C for 25 cycles.
  Lean periods (11 min): 500 ppm NO, 0.5% CO_2, 8% O_2 and 15 ppm SO_2.
  Rich periods (4 min): 500 ppm NO, 0.5% CO_2, 10,000 ppm H_2 and 15 ppm SO_2.

Long lean rich cycles were used in order to have a large breakthrough of NO_x. This is done to facilitate the modeling development. The catalyst was a monolith, which was 30 mm long and 21 mm in diameter. The catalyst was placed in a quartz tube with one thermocouple placed inside the catalyst and one about 1 cm in front of the sample. The gases were mixed using several mass flow controllers and the gases in the outlet feed stream was analyzed using a gas FTIR (MultiGas™ 2030). The total flow was 3500 ml/min which corresponds to a space velocity of 20,000 h^{-1}.

For the OSC measurements the catalyst was exposed to lean rich cycling. The gas composition was for lean conditions (11 min): 8% O_2, 0.5% CO_2, 15 ppm SO_2 and for rich conditions (4 min): 10,000 ppm H_2, 0.5% CO_2, 15 ppm SO_2. The first three cycles were sulfur free. The experiment was conducted at 300, 400 and 500 °C.

For the NO_x storage measurements cyclic experiments were conducted. 13 cycles were done in each experiment, with the first three free of sulfur. The gas composition was: Lean periods (11 min): 500 ppm NO, 0.5% CO_2, 8% O_2 and 15 ppm SO_2 and rich periods (4 min): 500 ppm NO, 0.5% CO_2, 10,000 ppm H_2 and 15 ppm SO_2. The catalyst was regenerated between each experiment with 500 ppm H_2 + 5% CO_2 for 60 min at 700 °C. The cycling at 400 °C, with the subsequent regeneration, was repeated in order to investigate the reproducibility. Further, cycling was also conducted at 300 and 500 °C, with regeneration at 700 °C using 500 ppm H_2 + 5% CO_2 for 60 min. Further, the effect of varying the regeneration was investigated. These experiments were followed by lean rich cycling experiments at 400 °C (same sequence as described above). The following regenerations were investigated: (i) 500 ppm H_2 + 5% CO_2 for 60 min at 700 °C, (ii) 500 ppm H_2 + 5% CO_2 for 60 min at 600 °C, (iii) 500 ppm H_2 + 5% CO_2 for 60 min at 500 °C, (iv) 500 ppm H_2 for 60 min at 700 °C, (v) 5000 ppm H_2 + 5% CO_2 for 60 min at 700 °C.

3. Catalyst model

The material balances were solved using FORTRAN.

The main governing equation for the gas phase species is:

$$\frac{w}{A_{tot}}\frac{\partial x_{g,i}}{\partial z} = -k_{m,i}S(x_{g,i} - x_{s,i}) = \sum_{j=1}^{nr} a_j s_{ij} r_j(T_s, c_s, \theta) \quad (1)$$

The coverage of component k on the surface is solved by:

$$\frac{d\theta_k}{dt} = \sum_{j=1}^{nr} s_{kj} r_j(T_s, c_s, \theta) \quad (2)$$

The relationship between the concentration and the molar fraction is:

$$c_{s,i} = c_{s,tot} x_{s,i} \quad (3)$$

where

$$c_{s,tot} = \frac{P_{tot}}{RT_s} \quad (4)$$

The film model is used to describe the mass-transfer between the gas and the catalyst surface, which is the middle term in Eq. (1) above. The mass-transfer coefficient was calculated using the Sherwood number (Sh = 3):

$$k_{m,i} = \frac{Sh}{D_h}(c_{g,tot} D_{i,m}) \quad (5)$$

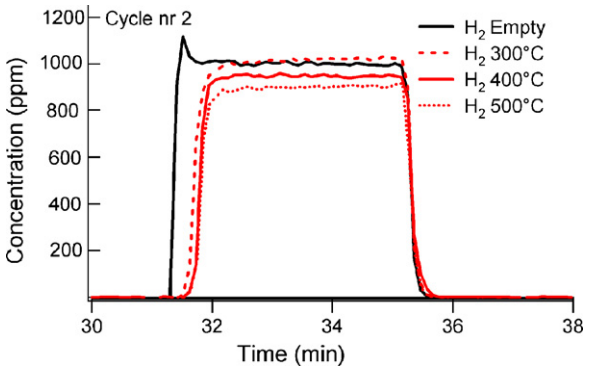

Fig. 1. The hydrogen concentration after OSC experiments at 300, 400 and 500 °C. Also the results from an empty reactor measurement are shown. The gas composition was for lean conditions (11 min): 8% O_2, 0.5% CO_2 and for rich conditions (4 min): 10,000 ppm H_2, 0.5% CO_2.

The geometric surface area per unit reactor volume, S, in Eq. (6) is given by:

$$\frac{S}{D_h} = 4 \times (\text{cell density}) \quad (6)$$

For the modeling of the NSR cycles, empty reactor measurements conducted at 400 °C were used as inlet data. A small reduction of the NO_x was observed in the presence of H_2 in the empty tube (about 10% without SO_2 and 3% with SO_2), which was compensated for in the model by using the inlet data. Also for the OSC simulations empty reactor measurements were used.

For the LNT experiments the temperature in the catalyst was used in the simulation and no heat balances were therefore solved. The temperature increase in the rich period was about 10 °C at 500 °C, less than 20 °C at 400 °C and less than 40 °C at 300 °C. The reason for the large difference in temperature increase is likely that the heat losses are much larger at higher temperatures. For the OSC simulations the temperature in the gas phase was used because the catalyst temperature was not measured in these experiments. However, since very similar experimental results were observed in the investigated temperature range (300–500 °C), see Fig. 1, the activation barrier is likely low. Therefore, possible temperature gradients will have small impact on the model.

3.1. The kinetic model

The Arrhenius equation is used to describe the rate constants, k:

$$k = Ae^{-E_A/RT_S} \quad (7)$$

3.1.1. Kinetic model for NO_x storage and regeneration

The total NO_x storage model contains several sub-models. The NO_x storage model was developed earlier using a shrinking core model [12,13]. In these experiments, conducted on a commercial catalyst [13], there was a long total uptake of NO_x, followed by a very slow increase of the NO_x that broke through. We suggested that the reason was the slow diffusion of NO_x into the particles. However, in the experiments conducted over the catalyst in this work the experimental results show a long total uptake and after that the NO_x concentration increases quite rapidly to the inlet value. One possible reason for this difference is that the newer commercial formulations may contain smaller barium particles for facilitating a larger and more rapid storage of NO_x. Due to these experimental results the shrinking core part of the model was not necessary and therefore not used in the rate for the storage. The rate and reaction rate for the storage of NO_x are found in Table 1. It is observed in many experimental investigations that NO_2 stores much more than NO [24] and therefore the rate was based on NO_2 adsorption, which is done in several other models [12,20,22]. Further, the NO oxidation of this sample was very high and it was therefore no need to introduce a reaction step for barium nitrite formation. However, this catalyst actually stores more NO_x at 300 °C compared to 400 °C. Thus it is important to add a low temperature storage component to the model, which has been done also in literature [22]. In temperature programmed desorption experiments it is observed multiple NO_x peaks for NO_x storage catalysts [25], and several authors propose that there are several types of NO_x storage sites present [25–31]. It is well known that alumina can adsorb significant amounts of NO_2. This has been observed using both flow reactor experiments [22,32] and in situ FTIR [31]. A study by Yi et al. [33] showed that 20 wt% barium gives about 0.75 mono layers. In addition, there is probably also barium particles formed which increases the available alumina surface. Thus, it is likely that there are alumina sites available also in our commercial sample and we have therefore added one reaction step for NO_2 storage on alumina. We have not investigated the storage on alumina in-depth and have therefore used a simple form of reaction for this process (r_2 in Table 1).

The NO oxidation is described by a reversible reaction and it is shown in Table 1 (r_3). Further, NO can be reduced to N_2 and also to NH_3 and this is described by reactions r_4 and r_5, respectively. For NO_x regeneration it is possible to form either NO_x components or N_2. Some steps must form NO_x, since a large NO_x peak is observed when switching to rich conditions. In a detailed kinetic model study [22] summary steps were used for NO_x regeneration, with a combination of formation of NO and N_2. In order to reduce the number of reaction steps this was also done in this work and the regeneration of the NO_x on barium and alumina are described in reaction r_6 and r_7. Further, in literature it is stated that an SCR reaction occurs between NO_x and the formed ammonia [22,34–37]. Lindholm et al. [22] found this step to be crucial in their detailed kinetic model in order to describe the delay in the ammonia signal when switching to rich conditions and simultaneously 100% conversion to NH_3 in the later part of the rich period. In that work a reaction step between

Table 1
Reaction and reaction rates for NO_x storage and regeneration.

Reaction description	Reaction	Reaction rate
NO_x storage on barium (r_1)	$0.5BaCO_3 + NO_2 + 0.25O_2 \overset{r_1}{\longleftrightarrow} 0.5Ba(NO_3)_2 + 0.5CO_2$	$r_1 = k_{\text{storage,Ba}} C_{NO_2} \theta_{BaCO_3} - k_{\text{decomposition,Ba}(NO_3)_2} C_{CO_2} \theta_{Ba(NO_3)_2}$
NO_x storage on alumina (r_2)	$Al_2O_3 + NO_2 \overset{r_2}{\longleftrightarrow} NO_2 - Al_2O_3$	$r_2 = k_{\text{storage,}Al_2O_3} C_{NO_2} \theta_{Al_2O_3} - k_{\text{decomposition,}Al_2O_3-NO_2} \theta_{Al_2O_3-NO_2}$
NO oxidation (r_3)	$NO + 0.5O_2 \overset{r_3}{\longleftrightarrow} NO_2$	$r_3 = k_{NO,ox} C_{NO} C_{O_2}^{0.5} - \frac{k_{NO,ox}}{K_{eq,NOox}} C_{NO_2}$
NO_x reduction (r_4)	$NO + H_2 \overset{r_4}{\longrightarrow} H_2O + 0.5N_2$	$r_4 = k_{NO,H_2} C_{NO} C_{H_2}$
NH_3 formation (r_5)	$NO + 2.5H_2 \overset{r_5}{\longrightarrow} NH_3 + H_2O$	$r_5 = k_{NH_3} C_{NO} C_{H_2}$
NO_x regeneration of barium (r_6)	$0.5Ba(NO_3)_2 + 1.5H_2 + 0.5CO_2 \overset{r_6}{\longrightarrow} 0.5BaCO_3 + 1.5H_2O + NO$	$r_6 = k_{\text{reg.,Ba}(NO_3)_2} C_{H_2} C_{CO_2} \theta_{Ba(NO_3)_2}$
NO_x regeneration of alumina (r_7)	$NO_2 - Al_2O_3 + 2H_2 \overset{r_7}{\longrightarrow} Al_2O_3 + 2H_2O + 0.5N_2$	$r_7 = k_{\text{reg.,}Al_2O_3-NO_2} C_{H_2} \theta_{Al_2O_3-NO_2}$
SCR between NH_3 and stored NO_x (r_8)	$1.5Ba(NO_3)_2 + 5NH_3 + 1.5CO_2 \overset{r_8}{\longrightarrow} 1.5BaCO_3 + 7.5H_2O + 4N_2$	$r_8 = k_{SCR} C_{NH_3} C_{CO_2} \theta_{Ba(NO_3)_2}$

Table 2
Reaction and reaction rates for oxygen storage and reduction.

Reaction description	Reaction	Reaction rate
Oxygen storage on S1 (r_9)	$Ce_2O_3(S1) + \frac{1}{2}O_2 \xrightarrow{r_9} 2CeO_2(S1)$	$r_9 = k_{ox,O_2,(S1)} C_{O_2} (1 - \theta_{S1.oxidised})$
Oxygen storage on S2 (r_{10})	$Ce_2O_3(S2) + \frac{1}{2}O_2 \xrightarrow{r_{10}} 2CeO_2(S2)$	$r_{10} = k_{ox,O_2,(S2)} C_{O_2} (1 - \theta_{S2.oxidised})$
Oxygen release from S1 (r_{11})	$2CeO_2(S1) + H_2 \xrightarrow{r_{11}} Ce_2O_3(S1) + H_2O$	$r_{11} = k_{red,H_2,S1} C_{H_2} \theta_{S1,oxidised}$
Oxygen release from S2 (r_{12})	$2CeO_2(S2) + H_2 \xrightarrow{r_{12}} Ce_2O_3(S2) + H_2O$	$r_{12} = k_{red,H_2,S2} C_{H_2} \theta_{S2,oxidised}$

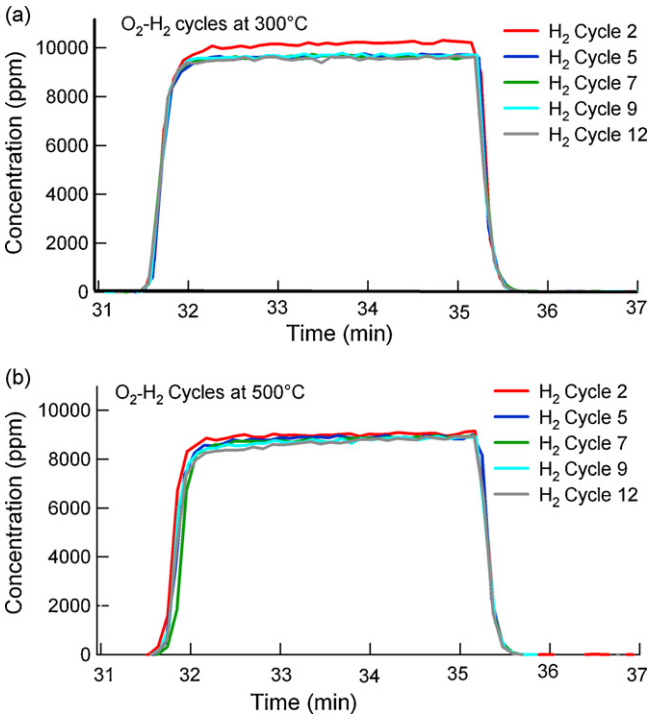

Fig. 2. A comparison between H_2 outlet signal for different cycle numbers in OSC experiments for (a) 300 °C and (b) 500 °C. The gas composition was for lean conditions (11 min): 8% O_2, 0.5% CO_2 and 15 ppm SO_2 and for rich conditions (4 min): 10,000 ppm H_2, 0.5% CO_2 and 15 ppm SO_2. The three first cycles are sulfur free.

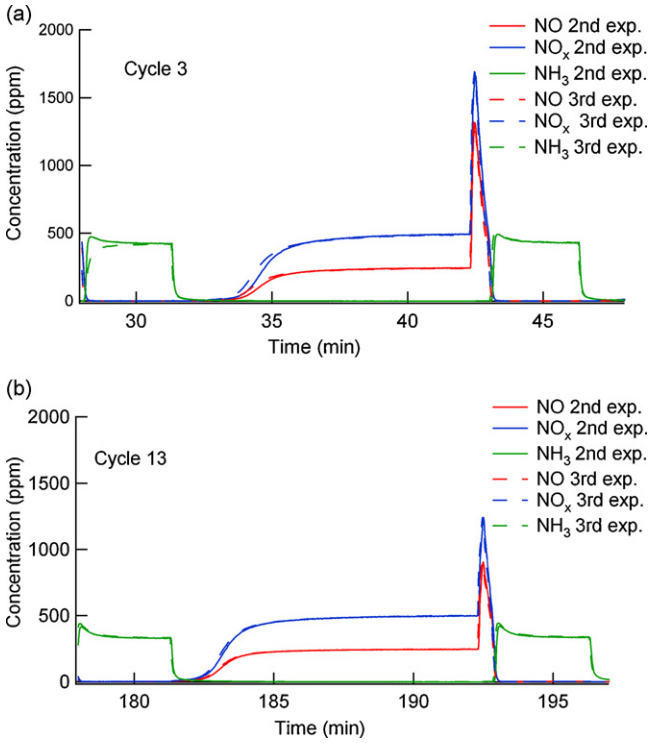

Fig. 3. NO_x Storage and Reduction cycles at 400 °C. The experiment was repeated and 2nd and 3rd experiments are shown. In (a) is cycle 3 shown and in (b) cycle 13. Lean periods (11 min): 500 ppm NO, 0.5% CO_2, 8% O_2 and 15 ppm SO_2. Rich periods (4 min): 500 ppm NO, 0.5% CO_2, 10,000 ppm H_2 and 15 ppm SO_2. For the first three cycles no SO_2 are present in the gas feed.

stored NO_x and ammonia was introduced. We have also included a summary step for this SCR reaction (r_8) in this study.

In the regeneration there are H_2 and CO_2 present simultaneously. CO will therefore be produced, due to the reverse water gas shift reaction. The reason for adding CO_2 to the experiments was to form $BaCO_3$ in the regeneration. We have used a low CO_2 concentration in order to limit the WGS reaction. We have measured WGS activity on a commercial TWC, which contained Pt, Rh and $CeZrO_x$. We used a similar space velocity and exposed the TWC to 5000 ppm H_2, 5% H_2O and 5% CO_2. We only observed a conversion of hydrogen of 0.1% and 1.4% at 200 and 300 °C, respectively. Even at 400 °C only 7% of the hydrogen was converted. Since we have a lower CO_2 concentration we expect the reverse WGS influence to be even less. In addition, we only observed CO production of 0.3% and 6% due to reverse WGS over a $Pt/Ba/Al_2O_3$ NO_x storage catalyst at 200 and 400 °C, respectively [38]. We have not added the WGS step to the model, which means that the kinetics for the regeneration is lumped for the combined effect of H_2 and CO, which was also done in an earlier publication [13]. However, as described above we believe that we only have small effects of reverse water gas shift during our conditions and that the dominating part of the regeneration is from hydrogen.

3.1.2. Kinetic model for oxygen storage and reduction

This commercial catalyst also contains oxygen storage materials and we have therefore added a model for describing this. We

Table 3
Reaction and reaction rates for sulfur poisoning and regeneration.

Reaction description	Reaction	Reaction rate
SO_2 adsorption on barium (r_{13})	$BaCO_3 + SO_2 \xleftrightarrow{r_{13}} BaCO_3 - SO_2$	$r_{13} = k_{Sulfur,ads,Ba} C_{SO_2} \theta_{BaCO_3} - k_{Sulfur,des,Ba} \theta_{BaCO_3-SO_2}$
Sulfate formation on barium (r_{14})	$BaCO_3 - SO_2 + 0.5O_2 \xrightarrow{r_{14}} BaSO_4 + CO_2$	$r_{14} = k_{BaSO_4,formation} C_{O_2} \theta_{BaCO_3-SO_2}$
SO_2 adsorption on alumina (r_{15})	$Al_2O_3 + SO_2 \xleftrightarrow{r_{15}} Al_2O_3 - SO_2$	$r_{15} = k_{Sulfur,ads,Al_2O_3} C_{SO_2} \theta_{Al_2O_3} - k_{Sulfur,des,Al_2O_3} \theta_{Al_2O_3-SO_2}$
Oxidation of SO_2 on alumina (r_{16})	$Al_2O_3 - SO_2 + 0.5O_2 \xrightarrow{r_{16}} Al_2O_3 - SO_3$	$r_{16} = k_{Al_2O_3-SO_3,formation} C_{O_2} \theta_{Al_2O_3-SO_2}$
Barium sulfate regeneration (r_{17})	$BaSO_4 + CO_2 + H_2 \xrightarrow{r_{17}} BaCO_3 + SO_2 + H_2O$	$r_{17} = k_{BaSO_4,reg.} C_{H_2} C_{CO_2} \theta_{BaSO_4}$
Alumina sulfate regeneration (r_{18})	$Al_2O_3 - SO_3 + H_2 \xrightarrow{r_{18}} Al_2O_3 + SO_2 + H_2O$	$r_{18} = k_{Al_2O_3-SO_3,reg.} C_{H_2} \theta_{Al_2O_3-SO_3}$

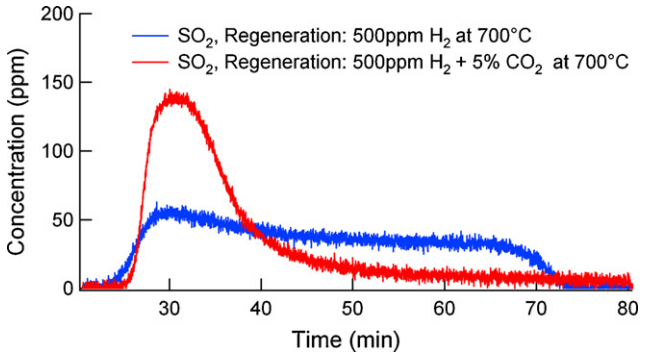

Fig. 4. Sulfur regeneration performed on the sulfur poisoned LNT catalyst with 500 ppm H_2 at 700 °C for 60 min or 500 ppm H_2 and 5% CO_2 at 700 °C for 60 min.

have earlier observed that on a TWC the reduction of the OSC is first very rapid and after that a slow process and we have used a two-site model to describe this. This was seen when using low concentrations of reductants. However, in this work we use high concentration of hydrogen (1%) and we cannot distinguish a fast and slow site, but to be consistent we also use a two-site model in this work. In the model reduced and oxidized ceria are used as sites, i.e. $CeO_{1.5}$ (=1/2 Ce_2O_3) and CeO_2, respectively. The reaction steps for the oxygen storage and regeneration are described in Table 2.

3.1.3. *Kinetic model for sulfur poisoning and regeneration*

The kinetic model for sulfur poisoning contains two steps on each storage site. First SO_2 is bond to the surface and after that oxidized. The main reason for this is that it has been observed earlier that when exposing the catalyst to SO_2 in the rich period also deactivates the catalyst [4]. Thus sulfur can adsorb on the catalyst without the presence of oxygen. However, we know that during lean period large quantities of sulfates are formed and it was therefore necessary to introduce one step on each site describing formation of sulfates (r_{13}–r_{16} in Table 3). In order not to complicate the model a simple form for the sulfate formation on alumina was added. The sulfates are regenerated to form H_2O and SO_2 by reactions with hydrogen (r_{17}–r_{18} in Table 3).

4. Results and discussion

4.1. *Sulfation of the OSC*

The oxygen storage capacity was investigated on the NO_x storage catalyst. Lean rich cycles were conducted without the presence of NO_x. The gas composition for lean conditions (11 min) was: 8% O_2, 0.5% CO_2 and for rich conditions (4 min): 10,000 ppm H_2, 0.5% CO_2. The experiment was conducted at 300, 400 and 500 °C. The hydrogen concentration out from the catalyst from cycle 2 is shown in Fig. 1 for all three temperatures. The results show that there are about 20 s of total removal of the hydrogen and that it is similar for all three temperatures. The reason for that the steady state level differs slightly between the temperatures is a calibration effect (calibration was conducted at one temperature). The lean rich cycles were repeated three times. This was followed by ten cycles with adding 15 ppm SO_2 to the gas mixture. In Fig. 2a the outlet hydrogen concentration is shown for cycle 2 (sulfur free), 5, 7, 9 and 12 at 300 °C. The corresponding experiments at 500 °C are shown in Fig. 2b. The results show that all cycles are similar, thus there are no sulfur poisoning observed for these two temperatures. The same

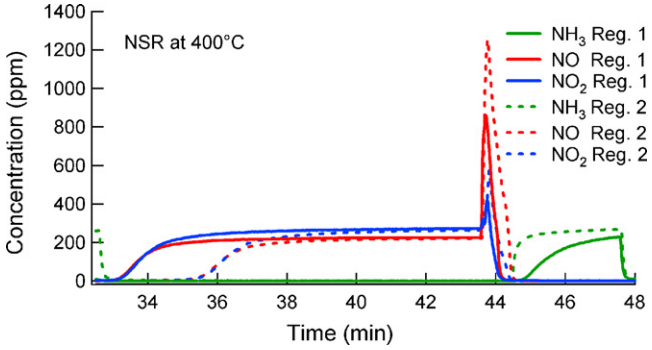

Fig. 5. Comparison between the third NSR cycle after different regeneration conditions. Regeneration 1: 500 ppm H_2 at 700 °C for 60 min. Regeneration 2: 500 ppm H_2 and 5% CO_2 at 700 °C for 60 min. Lean periods (11 min) are with 500 ppm NO, 8% O_2, 0.5% CO_2 and the rich periods (4 min) with 500 ppm NO, 10,000 ppm H_2, 0.5% CO_2.

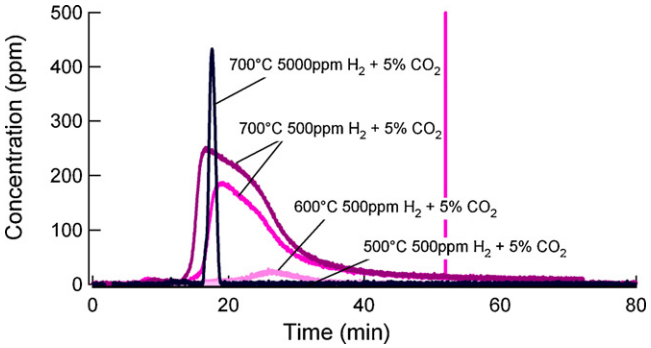

Fig. 6. Comparison of the SO_2 release at different regeneration conditions. Regeneration for 1 h at three different temperatures, 500, 600 and 700 °C with 500 pmm H_2 and 5% CO_2. Further, the effect of increasing the H_2 concentration to 5000 ppm was also examined at 700 °C.

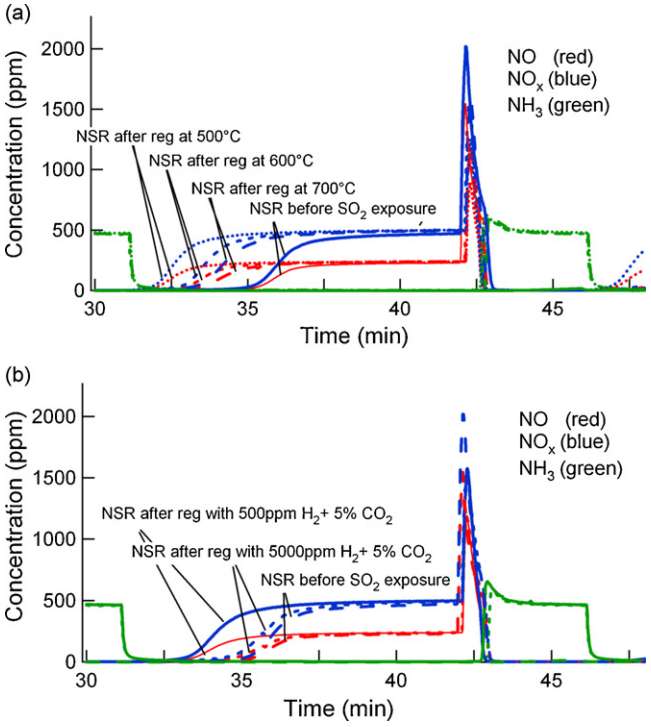

Fig. 7. Comparison between the storage cycle 3 performed at 400 °C after regeneration at (a) different temperatures 500, 600 and 700 °C and (b) different H_2 concentrations. The corresponding cycle performed on the catalyst before it ever had been exposed to sulfur is also shown. The regeneration conditions: 60 min with 500 pmm H_2 (or 5000 ppm) and 5% CO_2. Lean periods (11 min) with 500 ppm NO, 8% O_2, 0.5% CO_2 and 15 ppm SO_2. Rich periods (4 min) with 500 ppm NO, 10,000 ppm H_2, 0.5% CO_2 and 15 ppm SO_2. For the first three cycles no SO_2 is present.

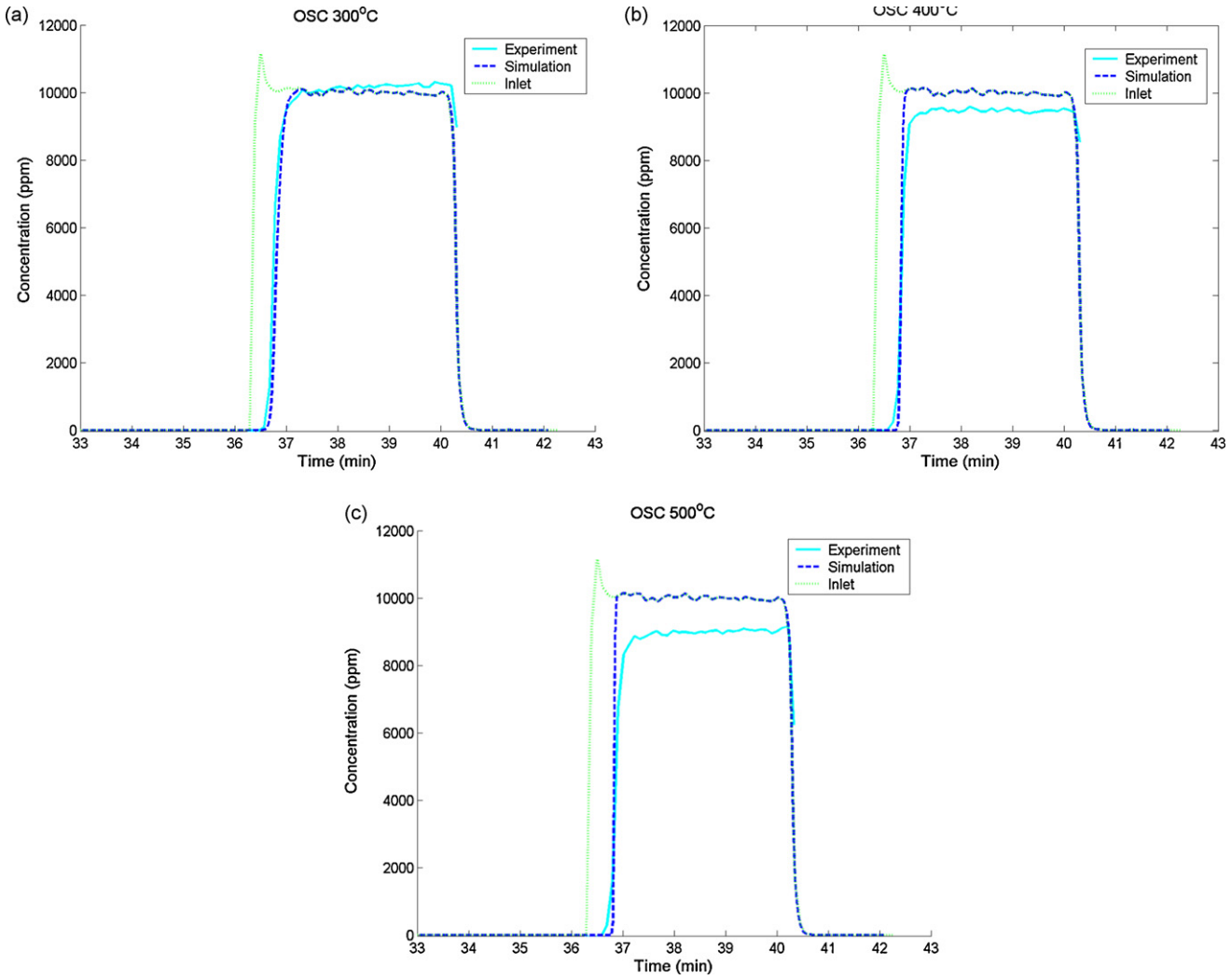

Fig. 8. Kinetic model for oxygen storage and reduction using hydrogen. The experiment and simulation is conducted at (a) 300 °C, (b) 400 °C and (c) 500 °C.

results were found also at 400 °C. No SO_2 is observed in the outlet. It is possible that there is sulfur storage in the lean period, which is removed in the rich period with a H_2S production, which we cannot detect with our instruments.

4.2. Sulfur poisoning and sulfur regeneration of lean NO_x traps

The sulfur poisoning was investigated using lean periods (11 min): 500 ppm NO, 0.5% CO_2, 8% O_2 and 15 ppm SO_2 and rich

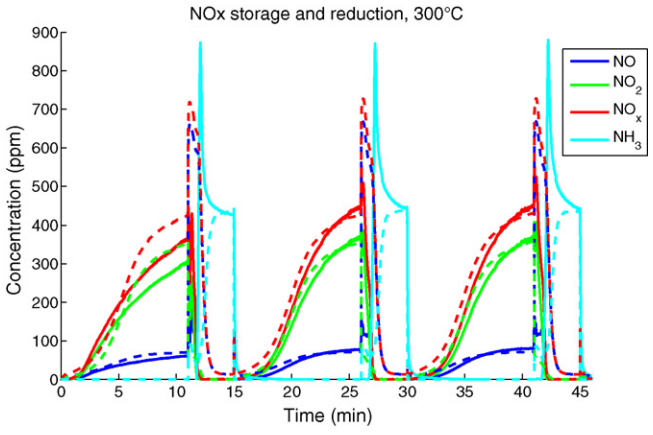

Fig. 9. Kinetic model for NO_x storage and reduction using hydrogen as reducing agent. The experiment and simulation is conducted at 300 °C. Solid lines: experiment. Dashed lines: simulation. Lean periods (11 min) with 500 ppm NO, 8% O_2, 0.5% CO_2. Rich periods (4 min) with 500 ppm NO, 10,000 ppm H_2, 0.5% CO_2.

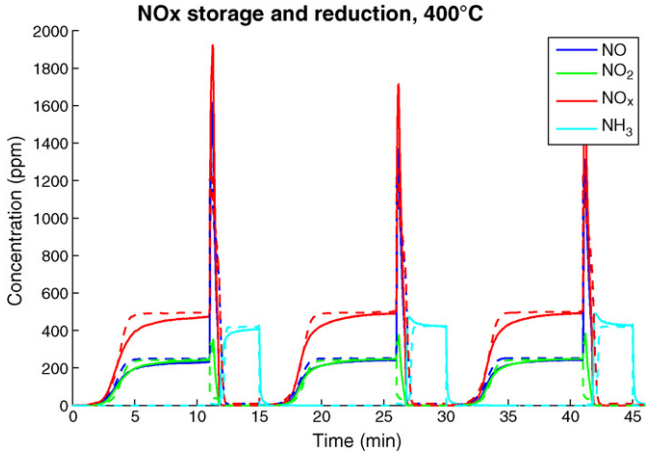

Fig. 10. Kinetic model for NO_x storage and reduction using hydrogen as reducing agent. The experiment and simulation is conducted at 400 °C. Solid lines: experiment. Dashed lines: simulation. Lean periods (11 min) with 500 ppm NO, 8% O_2, 0.5% CO_2. Rich periods (4 min) with 500 ppm NO, 10,000 ppm H_2, 0.5% CO_2.

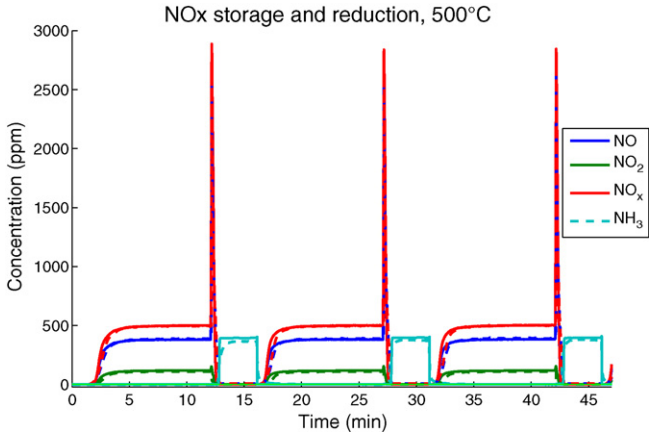

Fig. 11. Kinetic model for NO_x storage and reduction using hydrogen as reducing agent. The experiment and simulation is conducted at 500 °C. Solid lines: experiment. Dashed lines: simulation. Lean periods (11 min) with 500 ppm NO, 8% O_2, 0.5% CO_2. Rich periods (4 min) with 500 ppm NO, 10,000 ppm H_2, 0.5% CO_2.

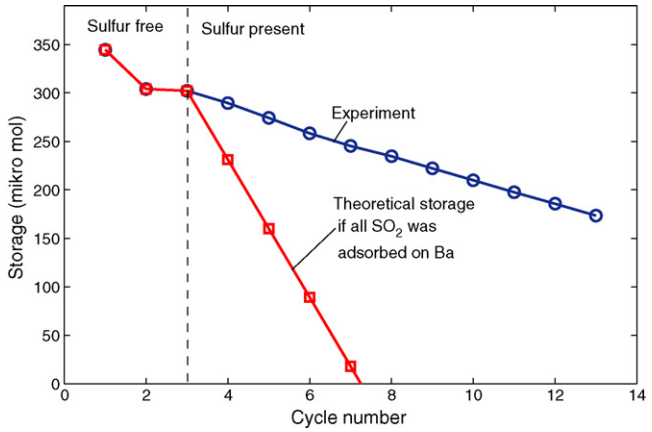

Fig. 12. Integrated NO_x storage capacity versus cycle number for an experiment conducted at 400 °C together with the theoretical storage capacity if all SO_2 adsorb on barium. Lean periods (11 min) with 500 ppm NO, 8% O_2 and 15 ppm SO_2. Rich periods (4 min) with 500 ppm NO, 10,000 ppm H_2 and 15 ppm SO_2. For the first three cycles no SO_2 is present.

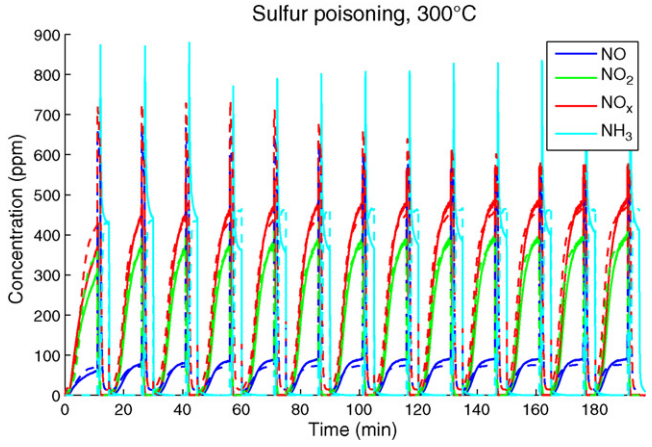

Fig. 13. Kinetic model for sulfur poisoning of NO_x storage and reduction using hydrogen as reducing agent. Lean periods (11 min) with 500 ppm NO, 8% O_2, 0.5% CO_2 and 15 ppm SO_2. Rich periods (4 min) with 500 ppm NO, 10,000 ppm H_2, 0.5% CO_2 and 15 ppm SO_2. For the first three cycles no SO_2 is present. The experiment and simulation is conducted at 300 °C. Solid lines: experiment. Dashed lines: simulation.

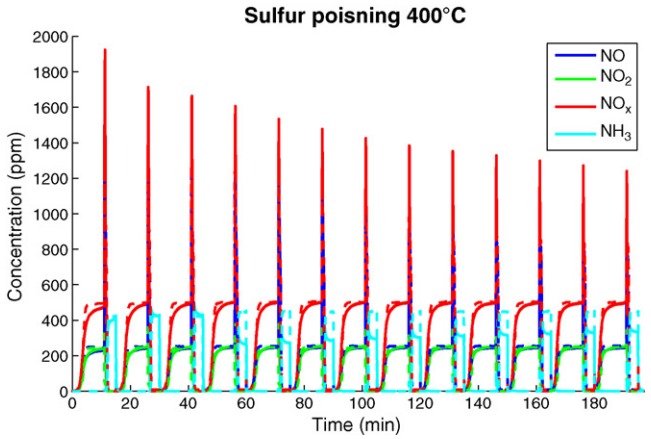

Fig. 14. Kinetic model for sulfur poisoning of NO_x storage and reduction using hydrogen as reducing agent. Lean periods (11 min) with 500 ppm NO, 8% O_2, 0.5% CO_2 and 15 ppm SO_2. Rich periods (4 min) with 500 ppm NO, 10,000 ppm H_2, 0.5% CO_2 and 15 ppm SO_2. For the first three cycles no SO_2 is present. The experiment and simulation is conducted at 400 °C. Solid lines: experiment. Dashed lines: simulation.

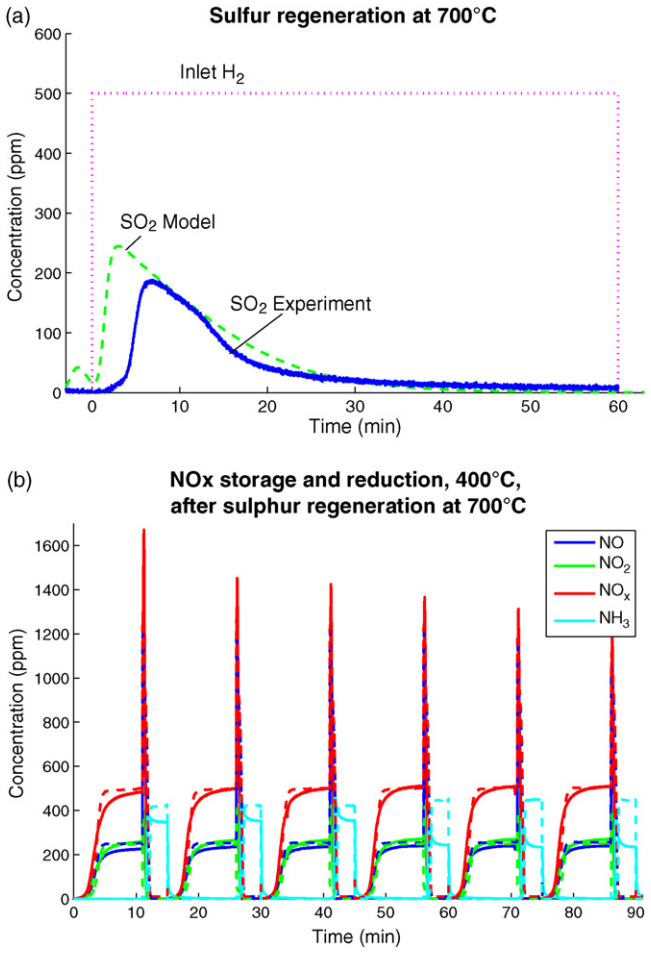

Fig. 15. (a) Kinetic model for sulfur regeneration at 700 °C with 500 ppm H_2 and 5% CO_2. (b) Kinetic model for NO_x storage cycles after sulfur regeneration shown in (a). Lean periods (11 min) with 500 ppm NO, 8% O_2, 0.5% CO_2 and 15 ppm SO_2. Rich periods (4 min) with 500 ppm NO, 10,000 ppm H_2, 0.5% CO_2 and 15 ppm SO_2. For the first three cycles no SO_2 is present. Solid lines: experiment. Dashed lines: simulation. The experiment and simulation is conducted at 400 °C.

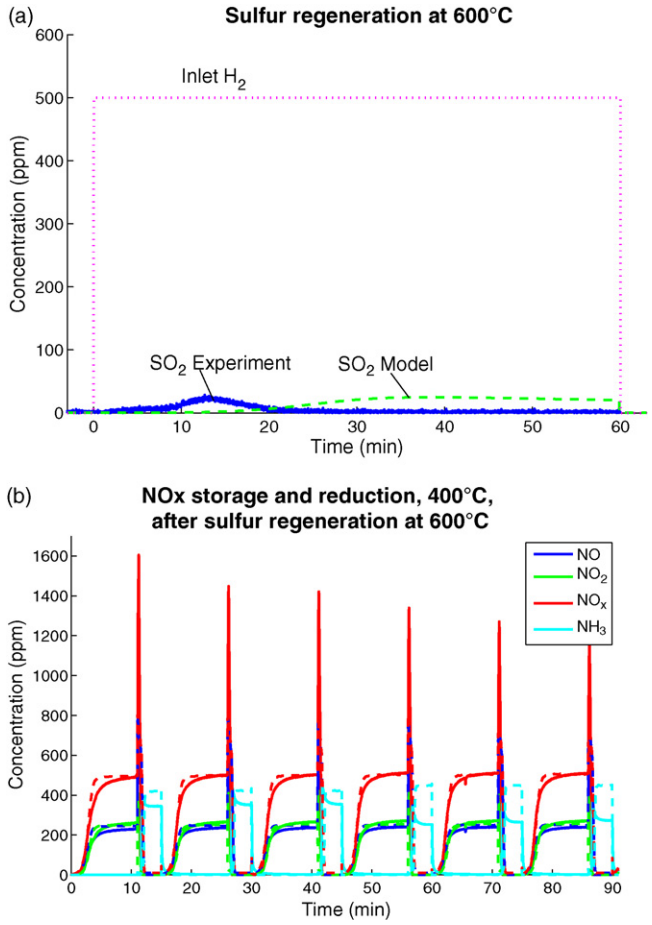

Fig. 16. (a) Kinetic model for sulfur regeneration at 600 °C with 500 ppm H_2 and 5% CO_2. (b) Kinetic model for NO_x storage cycles after sulfur regeneration shown in (a). Lean periods (11 min) with 500 ppm NO, 8% O_2, 0.5% CO_2 and 15 ppm SO_2. Rich periods (4 min) with 500 ppm NO, 10,000 ppm H_2, 0.5% CO_2 and 15 ppm SO_2. For the first three cycles no SO_2 is present. Solid lines: experiment. Dashed lines: simulation. The experiment and simulation is conducted at 400 °C.

periods (4 min): 500 ppm NO, 0.5% CO_2, 10,000 ppm H_2 and 15 ppm SO_2. The first three cycles were sulfur free. The results are shown in Fig. 3, where Fig. 3a shows a sulfur free cycle and Fig. 3b a cycle with sulfur. When the lean period starts there is a total uptake of NO_x and after that the NO_x breaks through and quite rapidly reaches the inlet values. When the rich period is started there is a large NO_x peak observed, due to incomplete regeneration of the stored NO_x. When the NO_x peak is close to zero ammonia formation is observed, showing a 100% selectivity of all incoming NO_x to form ammonia. After sulfur exposure (Fig. 3b) the total NO_x uptake is significantly reduced, which also results in a lower NO_x peak in the initial part of the reducing period. Further, the ammonia level is decreased in the presence of sulfur. Interestingly, the NO oxidation activity is not affected. Therefore it is likely that some sulfur species, possibly elemental sulfur, is adsorbed on the noble metal during the rich condition which decreases the ammonia production. These compounds are likely oxidized during the lean condition and the formed SO_2 is stored, which results in a high activity for NO oxidation. Further, the reproducibility of sulfur regeneration was also examined and in Fig. 3 the results from two experiments are shown, which were following regeneration with 500 ppm H_2 and 5% CO_2 at 700 °C for 60 min. The results clearly show that the experiments are reproducible.

In order to try to improve the regeneration CO_2 was added to the feed. The resulting SO_2 concentration from 60 min regeneration at 700 °C using 500 ppm H_2 only or 500 ppm H_2 and 5% CO_2 are shown in Fig. 4. When CO_2 is present there is a larger and more rapid release of SO_2. The results from cycling at 400 °C after sulfur regeneration with either H_2 or $H_2 + CO_2$ are shown in Fig. 5. The storage is increased dramatically when CO_2 was present during the regeneration. We suggest that the reason is that when CO_2 is present $BaCO_3$ will form and this compound is more stable than BaO. Thus, the formation of $BaCO_3$ increases the rate of decomposition of the sulfates.

The effect of varying the regeneration temperature and the hydrogen concentration was investigated and a comparison of the SO_2 released during the different regeneration conditions is shown in Fig. 6. It is clear that when increasing the temperature more SO_2 is released and that increasing the concentration of H_2 increases the rate of the regeneration drastically. For the regeneration at 700 °C using 500 ppm H_2 and 5% CO_2 there is one measuring point at about 52 min which is high (500 ppm). We believe that this is a measuring error. A comparison of NO_x storage cycles after the different regeneration temperatures is shown in Fig. 7a (Cycle 3, sulfur free). Increasing the regeneration temperature increases the regeneration and the subsequent NO_x storage. However, the storage capacity does not go back to the original state. The catalyst is exposed to about 350 μmols of SO_2 and during the rich condition to about 4700 μmols of H_2. Thus, there are 13 times more hydrogen available than the amount of SO_2 exposure. The maximum hydrogen consumption is obtained if all sulfates form H_2S (which is not the case) and that leads to that four times more hydrogen is needed compared to sulfur exposure. These results show that there are a large excess of hydrogen available also for the 500 ppm H_2 case, but the regeneration is anyhow not complete. In Fig. 7b (Cycle 3 sulfur free) is a comparison after the two different hydrogen concentrations and it is observed that when using the higher H_2 concentration the storage is almost back to the state before sulfur was introduced. Thus increasing temperature and concentration is very beneficial.

4.3. Kinetic model of oxygen storage over a commercial LNT catalyst

The kinetic model for oxygen storage was fitted to the experiments shown in Fig. 1. The catalyst was exposed to: lean conditions (11 min): 8% O_2, 0.5% CO_2 and rich conditions (4 min): 10,000 ppm H_2, 0.5% CO_2. These cycles were repeated three times and the second cycle was used in the simulations. The oxygen concentration in these experiments was chosen to 8%, which is the same as in the LNT experiments. However, since the concentration was high it was difficult to measure the actual oxygen uptake. The same barriers as for other simulations of OSC on TWC were applied for the oxidation of Ce_2O_3. The reduction of the CeO_2 was fitted and the results for experiments and kinetic model at 300, 400 and 500 °C are shown in Fig. 8. The reason for that the steady state level differs slightly between the temperatures is a calibration effect (calibration was conducted at one temperature). The results show that there is about 20 s of total removal of the hydrogen and that it is similar for all three temperatures. The model can describe the experiments adequately. There is a significant amount of hydrogen that is needed in order to reduce the OSC component, which influences the regeneration of the NO_x storage component. It is important to have a good model for the OSC in order to resolve the kinetics for the regeneration of the stored NO_x. There were no effect of sulfur poisoning on the OSC capacity at the investigated temperatures (Fig. 2), and sulfur poisoning was therefore not added to the model.

4.4. Kinetic model of NO_x storage and reduction over a commercial LNT catalyst

The storage and regeneration model was tuned to three experiments at 300, 400 and 500 °C, with the gas composition:

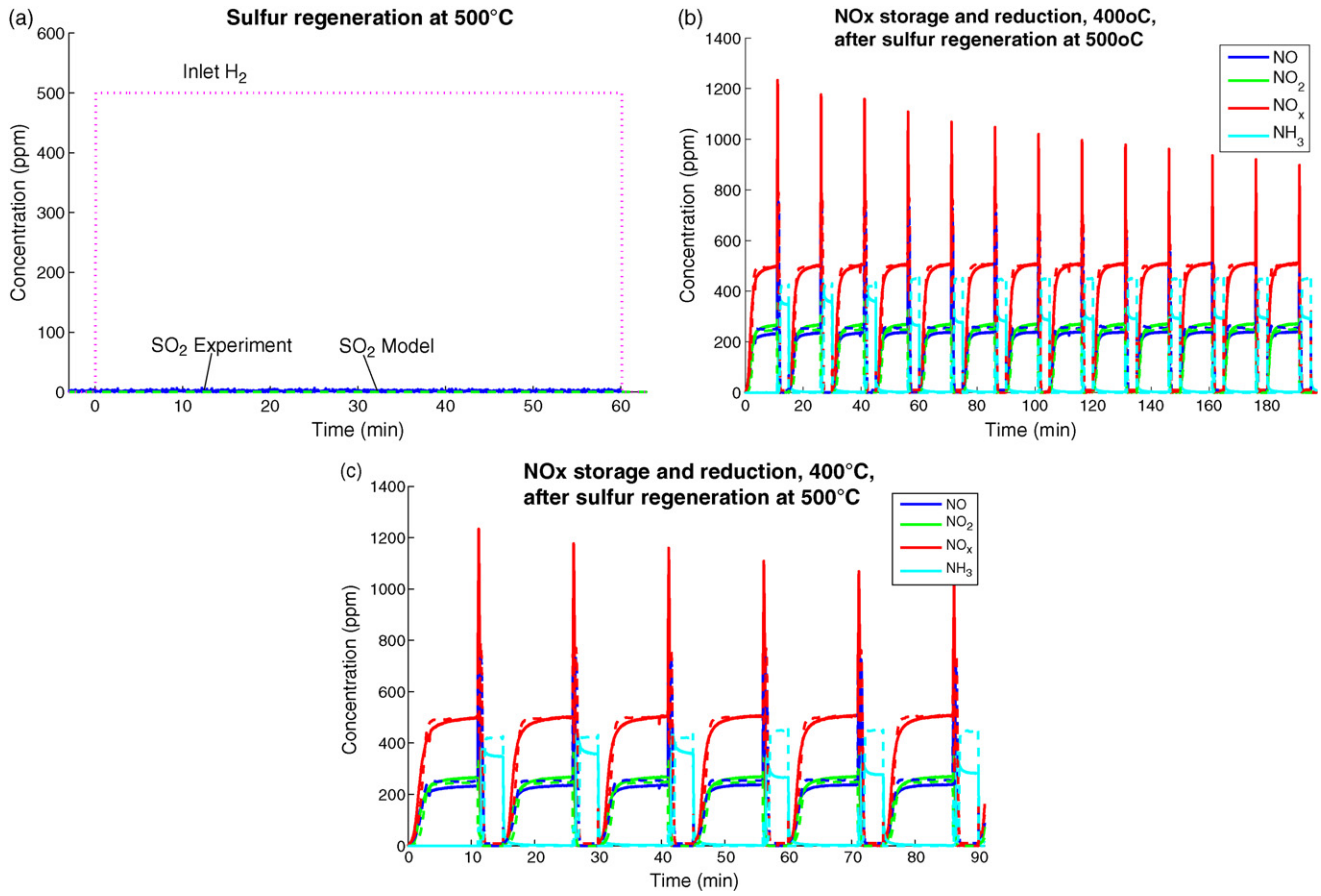

Fig. 17. (a) Kinetic model for sulfur regeneration at 500 °C with 500 ppm H_2 and 5% CO_2. (b) and (c) Kinetic model for NO_x storage cycles after sulfur regeneration shown in (a). Lean periods (11 min) with 500 ppm NO, 8% O_2, 0.5% CO_2 and 15 ppm SO_2. Rich periods (4 min) with 500 ppm NO, 10,000 ppm H_2, 0.5% CO_2 and 15 ppm SO_2. For the first three cycles no SO_2 is present. Solid lines: experiment. Dashed lines: simulation. The experiment and simulation is conducted at 400 °C.

Lean period (11 min): 500 ppm NO, 8% O_2, 0.5% CO_2
Rich periods (4 min): 500 ppm NO, 10,000 ppm H_2, 0.5% CO_2

The results from the model and experiment are shown in Figs. 9–11 for 300, 400 and 500 °C, respectively. Empty reactor measurements conducted at 400 °C were used as inlet data and the temperature in the catalyst was used in the simulations. The storage is largest at 300 °C, but is still significant also at 500 °C. The NO oxidation capacity of this sample is very high, also at 300 °C. The NO_x peaks in the initial part of the rich phase increases with increasing temperature, due to that the reaction rate for the regeneration of stored NO_x (r_6) increases with temperature. Ammonia is formed in the rich period. However, it is not observed until the NO_x peak has vanished. In the end of the rich period all the incoming NO_x is converted to ammonia. In order to describe the delay of the ammonia simultaneously with 100% selectivity towards ammonia in the later part of the rich period we suggest that there is an SCR reaction between stored NO_x and ammonia [22,34–37]. This is described by reaction r_5. The model can describe the experimental features adequately.

4.5. Kinetic model of sulfur poisoning of a NO_x storage catalyst

The sulfur poisoning was investigated at 300 and 400 °C using the following sequence: Lean periods (11 min) with 500 ppm NO, 8% O_2, 0.5% CO_2 and 15 ppm SO_2. Rich periods (4 min) with 500 ppm NO, 10,000 ppm H_2, 0.5% CO_2 and 15 ppm SO_2. For the first three cycles no SO_2 was present. The regeneration between the experiments was 60 min with 500 pmm H_2 and 5% CO_2 at 700 °C. The integrated NO_x storage versus cycle number is displayed in Fig. 12. It is clear that it is a linear poisoning that depends on the dose of sulfur, which also was observed by Amberntsson and co-workers [1]. If all sulfur in the inlet feed gas is assumed to be trapped on barium the theoretical NO_x storage capacity during sulfur poisoning can be calculated according to:

$$n_{\text{theoretical}} = n_{\text{cycle},3} - n_{SO_2} \cdot \text{no}_{\text{cycles}} \cdot 2 \quad (8)$$

This calculation is based on that the NO_x is adsorbed as $Ba(NO_3)_2$ and SO_2 as $BaSO_4$, i.e. two NO_x is adsorbed on each barium but only one SO_2. This is the reason for multiplying the sulfur exposure part with a factor of 2 in Eq. (8). The result from the theoretical NO_x storage capacity is also shown in Fig. 12. It is clear that the theoretical decrease has a much larger slope than the experiment. It is therefore likely that sulfur is adsorbed also on other sits. A barium loading of 20 wt% gives about 0.75 mono layers of barium coverage according to Yi et al. [33], thus to form one monolayer requires about 27 wt% barium. In addition, it is likely that barium also forms some particles which results in that an even higher barium loading is required to cover the surface. It is therefore probable that there are alumina sites available in our catalyst. Due to this we added a step for adsorption of NO_2 on alumina, which is described in the section Kinetic model for NO_x storage and regeneration. In the model we also added SO_2 adsorption to both $BaCO_3$ and also to the alumina sites. Significant amounts of SO_2 adsorption on alumina have been observed by Kylhammar et al. [39]. The NO_x stored on alumina is much more loosely bound compared to NO_x on barium. For example at 400 °C the NO_x storage is very low on alumina [40]. Therefore not all alumina sites are covered with NO_x at the tem-

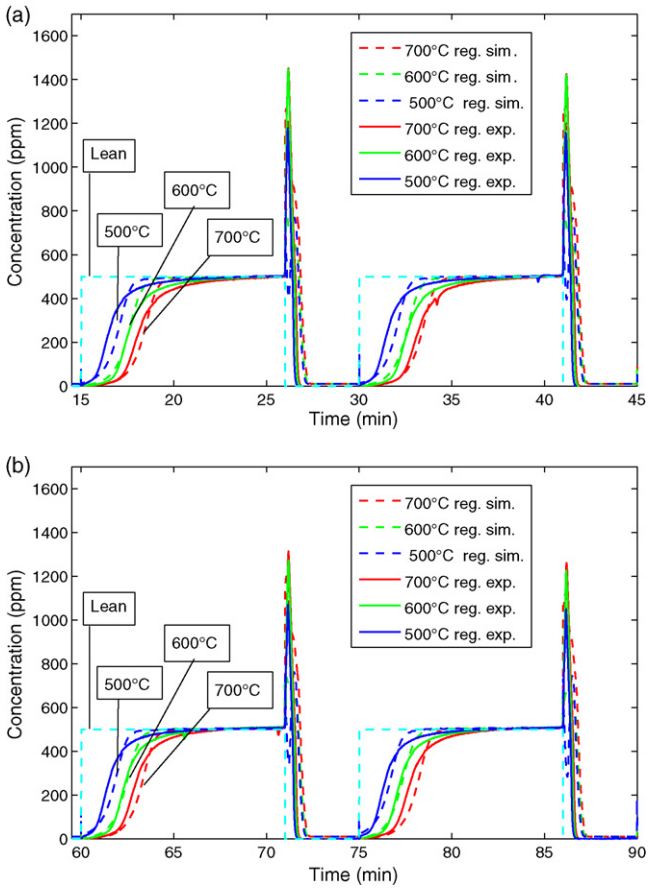

Fig. 18. Experiment and kinetic model for (a) cycle 2 and 3 (without sulfur) and (b) cycle 5 and 6 (with sulfur). Lean periods (11 min) with 500 ppm NO, 8% O_2 and 15 ppm SO_2. Rich periods (4 min) with 500 ppm NO, 10,000 ppm H_2 and 15 ppm SO_2. For the first three cycles no SO_2 is present. The experiment and simulation is conducted at 400 °C. Prior to the experiments are the catalyst regenerated from sulfur at 500, 600 or 700 °C. Solid lines: experiment. Dashed lines: simulation.

peratures investigated. However, sulfur binds strongly to alumina and can in the model be adsorbed on all alumina sites. Thus, many of the alumina sites that were not occupied by NO_x will adsorb SO_2. This feature is crucial for the sulfur poisoning model.

The results from the model and experiment for 13 lean rich cycles (first 3 are sulfur free) are shown in Fig. 13 and Fig. 14 for the temperatures 300 and 400 °C, respectively. The storage is reduced gradually during sulfur exposure, which the model described well. The addition of sulfur adsorption on alumina was crucial in order to describe the experimental observations and since no SO_2 was observed after the catalyst. The ammonia production is reduced when sulfur is present. This occurs instantly when sulfur is added and is likely due to sulfur deposits on the noble metal. We did not add reaction steps to describe this in the model. The NO_x peaks decreases gradually during the sulfur treatment, due to a smaller NO_x storage. The model can describe the experimental features well.

4.6. Kinetic model of sulfur regeneration of the NO_x storage catalyst

The effect of varying the sulfur regeneration temperature was modeled, using the reaction steps described in Table 3. The resulting SO_2 concentration from regeneration at 700 °C using 500 ppm H_2 and 5% CO_2 are shown in Fig. 15a. There is a large release of SO_2, both from the experiment and model. After this regeneration a cycling experiment was conducted at 400 °C, with: lean periods (11 min) with 500 ppm NO, 8% O_2, 0.5% CO_2 and 15 ppm SO_2 and rich periods (4 min) with 500 ppm NO, 10,000 ppm H_2, 0.5% CO_2 and 15 ppm SO_2. The first three cycles were sulfur free. The results for the first six cycles (first three are sulfur free) are shown in Fig. 15b. The corresponding results from regeneration at 600 °C are shown in Fig. 16 and for 500 °C in Fig. 17. There is a much smaller release of sulfur at 600 °C compared to at 700 °C. Further, no SO_2 is observed during regeneration at 500 °C. In Fig. 18 a comparison is shown for NO_x storage cycles at 400 °C after sulfur regeneration at 500, 600 and 700 °C. In Fig. 18a two sulfur free cycles are shown (cycle 2 and 3) and in Fig. 18b two cycles with 15 ppm SO_2 added (cycle 5 and 6). It is clear the NO_x storage capacity is decreased after regeneration at 600 °C compared to at 700 °C. When decreasing the regeneration temperature to 500 °C the NO_x storage is decreased even further. The model can describe the effect of regeneration temperature adequately.

5. Conclusions

Sulfur poisoning and regeneration of lean NO_x traps were investigated using experiments and kinetic modeling. A commercial Pt, Rh and barium containing commercial NO_x storage catalyst was used. The catalyst also contained oxygen storage material. The OSC was investigated using lean rich cycles with 8% O_2 and 1% H_2. A large OSC capacity was found and it was similar at all investigated temperatures (300, 400 and 500 °C). In addition, after three lean rich cycles 15 ppm SO_2 was added for another 10 cycles. No effect was observed by adding SO_2. However, we did not observe any SO_2 in the outlet feed gas during the cycling. It is possible that sulfur is stored on ceria during lean conditions, but is reduced during the hydrogen exposure, which results in the same consumption of hydrogen for all cycles. A two-site kinetic model was used for the OSC, which we have previously developed for TWC applications.

The sulfur poisoning of the NO_x storage was investigated using lean rich cycling experiments at 300, 400 and 500 °C. We observed that the NO_x storage decreased linearly when adding a constant level of SO_2. Further, the regeneration of 500 ppm H_2 for 60 min at 700 °C was not sufficient and the following NO_x cycles showed poor storage capacity. Interestingly, adding 5% CO_2 to the 500 ppm H_2 during the regeneration increased the storage capacity drastically. Thus, it is crucial with the formation of barium carbonates in order to remove the stored sulfur. Further, it was beneficial to increase the hydrogen concentration. Even though there was a large excess of hydrogen (more than four times than theoretically needed) when using 500 ppm H_2 + 5% CO_2, the regeneration was not complete. However, when using 5000 ppm H_2 + 5% CO_2 the regeneration was close to total. Thus, the rate for the regeneration is strongly dependent on the hydrogen concentration. Further, the regeneration was as expected decreased when decreasing the temperature.

The main objective with this work was to develop a kinetic model that can describe NO_x storage and regeneration, oxygen storage, sulfur poisoning during lean rich cycling and the regeneration of the formed sulfates. The kinetic model contains three sub-models: (i) NO_x storage and regeneration, (ii) oxygen storage and reduction and (iii) sulfur poisoning and sulfur regeneration. NO_x storage on two sites is crucial and we used storage on barium and alumina in the model. The NO_x adsorbed on alumina is more loosely bound and is important for low temperature storage. Alumina has been shown to store significant amounts of NO_x and that even with as high as 20 wt% barium only 0.75 of a monolayer can be formed, indicating available alumina sites. Reaction steps for NO oxidation, NO_x reduction and regeneration was also added, as well as ammonia formation. It was important to add an SCR step between stored NO_x and ammonia to describe the 100% selectivity to form ammonia simultaneously with that no ammo-

nia is observed during the initial part of the rich period. The sulfur submodel contains steps for adsorption of SO_2 on the two sites (barium and alumina) and the subsequent oxidation to form sulfates. If all sulfur would have been adsorbed only on barium the deactivation would have been to rapid. On alumina the NO_x is very loosely bound, resulting in low NO_x coverages at saturation at the temperatures investigated here (300, 400 and 500 °C). However, the sulfur binds strongly and can form high coverages of sulfates also on alumina. This result in that large quantity of sulfur can be adsorbed on alumina, with only a small reduction of the NO_x storage capacity. This effect was very important in order to describe the sulfur poisoning effect properly. In addition two reaction steps were added for describing the sulfur regeneration on barium and alumina. The model describes the experimental features well.

Acknowledgements

The work is performed at Competence Centre for Catalysis (KCK), Chalmers, GM Powertrain Sweden and at General Motors Research and Development Center. The authors would like to acknowledge helpful discussions with Se Oh, Ed Bissett, Jong-Hwan Lee, Byong Cho, Dave Monroe, Wei Li, Steven J. Schmieg of the General Motors Research and Development Center and Karthik Ramanathan at GM ISL and Annika Amberntsson and Maria Holmström at GM Powertrain Sweden. Ed Bissett is acknowledged for the GM fortran code for emission control simulations, which has been used in this work. We would also like to acknowledge Vinnova/Programrådet för fordonsforskning (Contract: P26789-1), GM Powertrain Sweden and GM R&D Center for the financial support. One author (Louise Olsson) would also like to acknowledge the Swedish Research Council (Contract: 621-2003-4149 and 621-2006-3706) and the Swedish foundation for strategic research (F06-0006) for additional support. The financial support for the reactor equipment from Knut and Alice Wallenberg Foundation, Dnr KAW 2005.0055, is gratefully acknowledged.

References

[1] P. Engstrom, A. Amberntsson, M. Skoglundh, E. Fridell, G. Smedler, Appl. Catal. B-Environ. 22 (1999) L241–L248.
[2] J. Dawody, M. Skoglundh, L. Olsson, E. Fridell, J. Catal. 234 (2005) 206–218.
[3] P.T. Fanson, M.R. Horton, W.N. Delgass, J. Lauterbach, Appl. Catal. B-Environ. 46 (2003) 393–413.
[4] H. Abdulhamid, E. Fridell, J. Dawody, M. Skoglundh, J. Catal. 241 (2006) 200–210.
[5] C. Sedlmair, K. Seshan, A. Jentys, J.A. Lercher, 3rd European Workshop on Environmental Catalysis, Elsevier Science Bv, Maiori, Italy, 2001, pp. 413–419.
[6] Y. Su, M.D. Amiridis, Catal. Today 96 (2004) 31–41.
[7] S. Poulston, R.R. Rajaram, Catal. Today 81 (2003) 603–610.
[8] H. Mahzoul, L. Limousy, J.F. Brilhac, P. Gilot, J. Anal. Appl. Pyrolysis 56 (2000) 179–193.
[9] K. Yamazaki, T. Suzuki, N. Takahashi, K. Yokota, M. Sugiura, Appl. Catal. B-Environ. 30 (2001) 459–468.
[10] A. Amberntsson, M. Skoglundh, S. Ljungstrom, E. Fridell, J. Catal. 217 (2003) 253–263.
[11] E.C. Corbos, S. Elbouazzaoui, X. Courtois, N. Bion, P. Marecot, D. Duprez, Top. Catal. 42–43 (1–4) (2007) 9.
[12] L. Olsson, R.J. Blint, E. Fridell, Ind. Eng. Chem. Res. 44 (2005) 3021–3032.
[13] L. Olsson, D. Monroe, R.J. Blint, Ind. Eng. Chem. Res. 45 (2006) 8883–8890.
[14] U. Tuttlies, V. Schmeisser, G. Eigenberger, Chem. Eng. Sci. 59 (2004) 4731–4738.
[15] C.M.L. Scholz, V.R. Gangwal, M. de Croon, J.C. Schouten, J. Catal. 245 (2007) 215–227.
[16] F. Laurent, C.J. Pope, H. Mahzoul, L. Delfosse, P. Gilot, Chem. Eng. Sci. 58 (2003) 1793–1803.
[17] P. Koci, F. Plat, J. Stepanek, M. Kubicek, M. Marek, Catal. Today 137 (2008) 253.
[18] D. Bhatia, R.D. Clayton, M.P. Harold, V. Balakotaiah, Catal. Today 147 (2009) S250–S256.
[19] P. Koci, F. Plat, J. Stepanek, S. Bartova, M. Marek, M. Kubicek, V. Schmeisser, D. Chatterjee, M. Weibel, Catal. Today 147 (2009) S257–S264.
[20] L. Olsson, H. Persson, E. Fridell, M. Skoglundh, B. Andersson, J. Phys. Chem. B 105 (2001) 6895.
[21] L. Olsson, E. Fridell, M. Skoglundh, B. Andersson, Catal. Today 73 (2002) 263–270.
[22] A. Lindholm, N.W. Currier, J. Li, A. Yezerets, L. Olsson, J. Catal. 258 (2008) 273.
[23] J. Dawody, M. Skoglundh, L. Olsson, E. Fridell, Appl. Catal. B-Environ. 70 (2007) 179–188.
[24] E. Fridell, M. Skoglundh, B. Westerberg, S. Johansson, G. Smedler, J. Catal. 183 (1999) 196–209.
[25] A. Lindholm, N.W. Currierc, J. Dawody, A. Hidayata, J. Li, A. Yezerets, L. Olsson, Appl. Catal. B: Environ. 88 (2009) 240.
[26] H. Mahzoul, J.F. Brilhac, P. Gilot, Appl. Catal. B-Environ. 20 (1999) 47–55.
[27] W.S. Epling, J.E. Parks, G.C. Campbell, A. Yezerets, N.W. Currier, L.E. Campbell, Catal. Today 96 (2004) 21–30.
[28] D. James, E. Fourre, M. Ishii, M. Bowker, Appl. Catal. B-Environ. 45 (2003) 147–159.
[29] L. Lietti, P. Forzatti, I. Nova, E. Tronconi, J. Catal. 204 (2001) 175–191.
[30] J.H.K.J. Szanyi, D.H. Kim, S.D. Burton, C.H. Peden, J. Phys. Chem. B Lett. 109 (2005) 27–29.
[31] B. Westerberg, E. Fridell, J. Mol. Catal. A-Chem. 165 (2001) 249–263.
[32] E. Fridell, H. Persson, B. Westerberg, L. Olsson, M. Skoglundh, Catal. Lett. 66 (2000) 71–74.
[33] C.-W. Yi, J.H. Kwak, C.H.F. Peden, C. Wang, J. Szanyi, J. Phys. Chem. C Lett. 111 (2007) 14942.
[34] L. Cumaranatunge, S.S. Mulla, A. Yezerets, N.W. Currier, W.N. Delgass, F.H. Ribeiro, J. Catal. 246 (2007) 29–34.
[35] J.A. Pihl, J.E. Parks, C. Stuart Daw, T.W. Root, SAE Tech. Paper 2006-01-3441 (2006).
[36] I. Nova, L. Lietti, P. Forzatti, Catal. Today 136 (2008) 128.
[37] S.S. Mulla, S.S. Chaugule, A. Yezerets, N.W. Currier, W.N. Delgass, F.H. Ribeiro, Catal. Today 136 (2008) 136.
[38] A. Lindholm, H. Sjövall, L. Olsson, Appl. Catal. B: Environ. 98 (2010) 112.
[39] L. Kylhammar, P.A. Carlsson, H.H. Ingelsten, H. Gronbeck, M. Skoglundh, Appl. Catal. B-Environ. 84 (2008) 268–276.
[40] A. Lindholm, N.W. Currier, E. Fridell, A. Yezerets, L. Olsson, Appl. Catal. B: Environ. 75 (2007) 78.